J Mol Model (2012) 18:4675–4686
DOI 10.1007/s00894-012-1467-3

ORIGINAL PAPER

Photodissociation of a ruthenium(II) arene complex and its subsequent interactions with biomolecules: a density functional theory study

Hanlu Wang · Nathan J. DeYonker · Xiting Zhang · Cunyuan Zhao · Liangnian Ji · Zong-Wan Mao

Received: 3 February 2012 / Accepted: 13 May 2012 / Published online: 1 June 2012

Abstract The piano-stool Ru^{II} arene complex $[(\eta^6\text{-benz})Ru(bpm)(py)]^{2+}$ (benz=benzene, bpm=2,2′-bipyrimidine, and py=pyridine), which is conventionally nonlabile (on a time-scale and under conditions relevant for biological reactivity), can be activated by visible light to selectively photodissociate the monodentate ligand (py). In the present study, the aquation and binding of the photocontrolled ruthenium(II) arene complex $[(\eta^6\text{-benz})Ru(bpm)(py)]^{2+}$ to various biomolecules are studied by density functional theory (DFT) and time-dependent DFT (TDDFT). Potential energy curves (PECs) calculated for the Ru–N (py) bonds in $[(\eta^6\text{-benz})Ru(bpm)(py)]^{2+}$ in the singlet and triplet state give useful insights into the photodissociation mechanism of py. The binding energies of the various biomolecules are calculated, which allows the order of binding affinities among the considered nuleic-acid- or protein-binding sites to be discerned. The kinetics for the replacement of water in the aqua complex with biomolecules is also considered, and the results demonstrate that guanine is superior to other biomolecules in terms of coordinating with the Ru^{II} aqua adduct, which is in reasonable agreement with experimental observations.

Keywords Ruthenium · Arene complex · Anticancer drugs · Photodissociation · Density functional theory

Abbreviations

bpm	2,2′-Bipyrimidine
Ru-bpm	$[(\eta^6\text{-benz})Ru^{II}(bpm)]^{2+}$
p-cym	*p*-Cymene
benz	Benzene
G	Guanine
py	Pyridine
A	Adenine
met	$(CH_3)_2S$
cys	CH_3SH
cym-Ru-py	$[(\eta^6\text{-}p\text{-cym})Ru^{II}(bpm)(py)]^{2+}$
Ru-py	$[(\eta^6\text{-benz})Ru^{II}(bpm)(py)]^{2+}$
Ru-H_2O	$[(\eta^6\text{-benz})Ru^{II}(bpm)(H_2O)]^{2+}$
Ru-G	$[(\eta^6\text{-benz})Ru^{II}(bpm)(G)]^{2+}$
Ru-A	$[(\eta^6\text{-benz})Ru^{II}(bpm)(A)]^{2+}$
Ru-hist	$[(\eta^6\text{-benz})Ru^{II}(bpm)(hist)]^{2+}$
Ru-cys	$[(\eta^6\text{-benz})Ru^{II}(bpm)(cys)]^{2+}$
Ru-met	$[(\eta^6\text{-benz})Ru^{II}(bpm)(met)]^{2+}$
hist	5-Methyl-1H-imidazole

Introduction

Apart from cisplatin and some derivatives, successful metallopharmaceuticals are still scarce in antitumor therapy [1, 2]. Despite the fact that novel metal complexes have been investigated in preclinical settings, several promising compounds failed during subsequent phases. With the rise of new anticancer compounds, new activation strategies have also evolved [3, 4]. Photochemical activation is a new concept where prodrug activity

Electronic supplementary material The online version of this article (doi:10.1007/s00894-012-1467-3) contains supplementary material, which is available to authorized users.

H. Wang · X. Zhang · C. Zhao (✉) · L. Ji · Z.-W. Mao (✉)
MOE Key Laboratory of Bioinorganic and Synthetic Chemistry/KLGHEI of Environment and Energy Chemistry, School of Chemistry and Chemical Engineering, Sun Yat-Sen University, Guangzhou 510275, People's Republic of China
e-mail: ceszhcy@mail.sysu.edu.cn
e-mail: cesmzw@mail.sysu.edu.cn

N. J. DeYonker
Department of Chemistry, The University of Memphis, Memphis, TN 38152-3550, USA

can be triggered by light. This strategy offers the possibility of controlling the location, timing, and dosage of the therapeutic metal complex. Photoreactions are characterized by a loss of a monodentate ligand and the coordination of a solvent molecule. In nonpolar solvents, the solvent molecule is replaced through the coordination of counterions, added ions, or residual water [5–8].

Organometallic ruthenium complexes bearing a π-bonded arene ligand are considered promising candidates for cancer treatment. Complexes bearing the ethylenediamine (en) ligand show cytotoxicity comparable to that of the clinically used drugs cisplatin and carboplatin [9, 10]. On the other hand, compounds containing phosphatriazaadamantane (pta) or its derivatives have been developed that show antimetastatic activity but low cytotoxicity in vitro [11, 12]. Recently, a class of organoruthenium compounds considered as an alternative to cisplatin has been studied in detail [13]. Some theoretical studies of Ru(II) complexes intercalated in DNA have also been reported [14–16]. DNA platination plays an important role in the mechanism of action of platinum anticancer drugs such as cisplatin, whereas the interaction of platinum species with S-containing biomolecules has been associated with both negative phenomena (such as toxic side effects and the development of resistance) and positive effects (such as the delivery of active species to cells and/or their capacity to serve as a drug reservoir for ultimate platination of DNA) [17, 18]. DNA is a potential target for en-Ru^{II}-arene complexes, and they exhibit a high selectivity for binding to N7 of guanine [19–21]. Ruthenium-arene complexes that bind to sulfur (S-donor/thiolate) compounds have also been observed, but the resulting complexes are often kinetically unstable, especially in the presence of oxygen [22, 23].

We have been intrigued by the photochemical properties of organometallic $[(\eta^6\text{-}p\text{-cymene})Ru(bpm)(py)]^{2+}$ complexes synthesized and studied by Sadler and co-workers [24–26]. In a recent paper, the authors studied the in vitro photorelease of pyridine from the complex $[(\eta^6\text{-}p\text{-cymene})Ru(bpm)(py)]^{2+}$ upon excitation with visible white light (400–600 nm, 1 Jcm^{-2} h^{-1}). Furthermore, they improved the selectivity of $[(\eta^6\text{-}p\text{-cym})Ru(bpm)(py)]^{2+}$ against cancer cells based on the covalent attachment of a delivery peptide through the pyridine ligand. These peptides can act as "tumor-targeting devices," since their receptors are overexpressed on the membranes of tumor cells. Why guanine eventually wins the competition for the coordination sites of the Ru-bpm derivatives against other nucleobases and peptides containing cysteine or methionine side chains is not well understood [26]. Sadler and coauthors ascribed this predominance for guanine to the steric hindrance created by the covalent bond between the peptide and the oligonucleotide chain. Our computations suggested that binding to guanine is also kinetically preferred over peptides.

The objective of the DFT study described in this paper was to investigate the reactivity of the ruthenium–ligand bond in this photocontrolled complex, $[(\eta^6\text{-benz})Ru(bpm)(py)]^{2+}$; see Fig. 1. In ruthenium-arene complexes, the character of the arene has limited influence on the kinetics of the aquation [27, 28], but it does have a significant influence on the kinetics of the binding to DNA. For example, complexes with extended π-electron systems as well as coordination to guanine and noncoordinative, hydrophobic interactions between the arene ligand and DNA can occur [29, 30]. These may include arene–base stacking, arene intercalation, and minor-groove binding, and are thought to contribute to the driving force for the binding of chloro-Ru^{II}-arene complexes to double-helical DNA [29, 30]. As this study focuses on the relative reactivity of the complex towards biomolecules, the *p*-cymene ligand in the model complex was simplified to a benzene ligand.

In the present work, we first described the optimized structures of the complex and the biomolecule adducts $[(\eta^6\text{-benz})Ru(bpm)L]^{2+}$, where L is a neutral ligand such as pyridine (py), H_2O, guanine (G), adenine (A), 5-methyl-1H-imidazole (hist, representing the functional group—imidazole—of histidine), CH_3SH (cys, representing the functional group—thiol—of cysteine), or $(CH_3)_2S$ (met, representing the functional group—thioether—of methionine). We then analyzed the photophysical and photochemical features of $[(\eta^6\text{-benz})Ru(bpm)(py)]^{2+}$. The aim of this work was to explore the formation of the reactive aqua species upon irradiation. Finally, the binding of the various biomolecules to the complex was calculated, which allowed us to discern the binding affinity order for the considered ligands. Furthermore, the kinetics and thermodynamics of the reactions of the solvated species with various biomolecules in the cell were investigated.

Computational methods

The compounds $[(\eta^6\text{-benz})Ru(bpm)L]^{2+}$, (benz=benzene, bpm=2,2′-bipyrimidine, L=pyridine (py), H_2O, guanine (G), adenine (A), 5-methyl-1H-imidazole (hist), CH_3SH (cys), $(CH_3)_2S$ (met)) were examined as shown in Fig. 1, where a pseudo-octahedral arrangement of the Ru is assumed. Geometry optimizations without symmetry constraints in water (ε=78.35) were performed, employing DFT with Becke's three-parameter hybrid functional [31] and Lee–Yang–Parr's gradient-corrected correlation functional [32] (B3LYP), which has been demonstrated to be effective for the calculation of Ru-arene complexes [25, 27, 28, 33, 34]. The LanL2DZ basis set [35] and effective

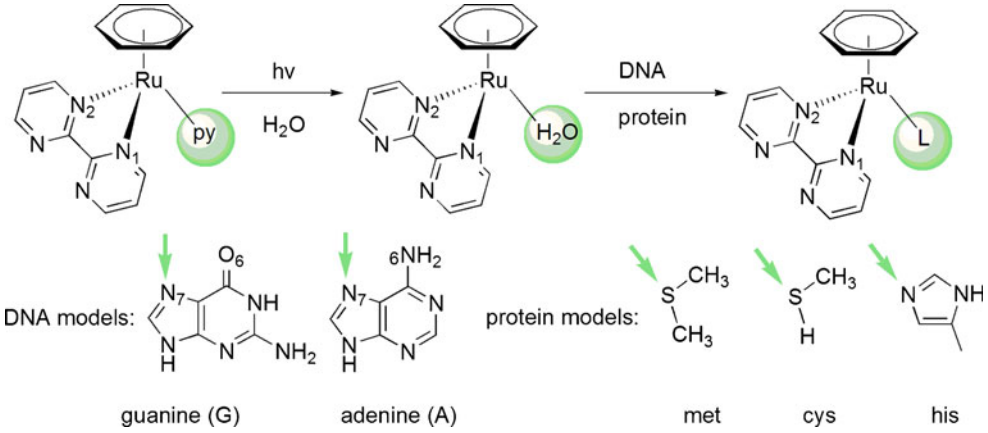

Fig. 1 Photoinduced aquation and biomolecular substitution reaction of $[(\eta^6\text{-benz})M(bpm)(py)]^{2+}$

core potential were used for the Ru atom, and the split-valence 6-31 G** basis set was applied for all other atoms [36]. The solvent effects of water were taken into account via the COSMO implicit solvent approach [37, 38]. Thermal energies were extracted from vibrational frequency calculations, which were used to verify the nature of the stationary points at 298.15 K and 1 atm (in vacuum). Frequency calculations also served to confirm the character of the transition-state (TS) structures as well as the reactant and product (super) molecules.

The characterization of the nature of the lowest-lying singlet and triplet excited states of cym-Ru-py and Ru-py involved in absorption and emission properties, respectively, relied on time-dependent density functional theory (TDDFT) [39, 40]. Single-point calculations combined with the COSMO method were performed for the ground-state optimized geometry. Thirty-two singlet excited states and eight triplet excited states were determined starting from the ground-state geometries. Our approach was motivated by previous works in which the electronic and optical properties of ruthenium complexes calculated by TDDFT were in reasonable agreement with those measured experimentally [41, 42]. The theoretical UV curves were obtained using the program GaussSum-2.2.2 [43].

The effects of Ru–N3(py) bond elongation on the singlet and triplet states were studied computationally by TDDFT employing the ground-state geometries. Starting from the ground-state minimum, the Ru–N3(py) distances were varied independently by 0.1 Å. In each step, the Ru–N3 (py) bond distance was frozen and the geometry of the molecule was allowed to relax to a constrained stationary point. Each point was then used to calculate 32 vertical singlet excited states and eight vertical triplet excited states via TDDFT at the B3LYP/6-31 G** (LanL2DZ for Ru) level.

Binding energies of ligands in ruthenium complexes can be predicted and rationalized using density functional theory (DFT) methods [27, 33, 34]. The binding energies for benz and L in Ru^{II}-arene complexes were calculated in an attempt to rationalize the experimental observations. All of the fragments were reoptimized in water solution. Binding energies were obtained using the general formulae

$$\Delta E_{\mathrm{Ru-benz}} = E_{[\mathrm{Ru(bpm)L}]^{2+}} + E_{(\mathrm{benz})} - E_{[(\eta^6-\mathrm{benz})\mathrm{Ru(bpm)L}]^{2+}} \quad (1)$$

$$\Delta E_{\mathrm{Ru-L}} = E_{[(\eta^6-\mathrm{benz})\mathrm{Ru(bpm)}]^{2+}} + E_{(\mathrm{L})} - E_{[(\eta^6-\mathrm{benz})\mathrm{Ru(bpm)L}]^{2+}}, \quad (2)$$

where L=H_2O, py, cys, met, hist, G, or A.

All calculations were performed with the Gaussian09 package [44].

Results and discussion

For readability, simple acronyms are used throughout this section instead of the full chemical formulae with ligand abbreviations. Definitions of the abbreviations used are displayed in the "Electronic supplementary material" (ESM).

Structural characteristics

The gas-phase and COSMO distances of the metal–ligand coordination bonds in complexes with biomolecules are presented in Fig. 2. The key bond lengths of Ru-py are very similar to those of cym-Ru-py, suggesting that the alkyl ligand in the arene has only a limited effect on the structural and electronic properties of the complex. The Ru–N1 and Ru–N2 distances shorten slightly upon moving from gas-phase to the continuum model for all the complexes. The Ru–arene [represented as the average of the Ru–C(benz) lengths] distances also shorten slightly when changing from gas-phase calculations to those performed with the COSMO continuum model, reflecting the hydrophobic character of

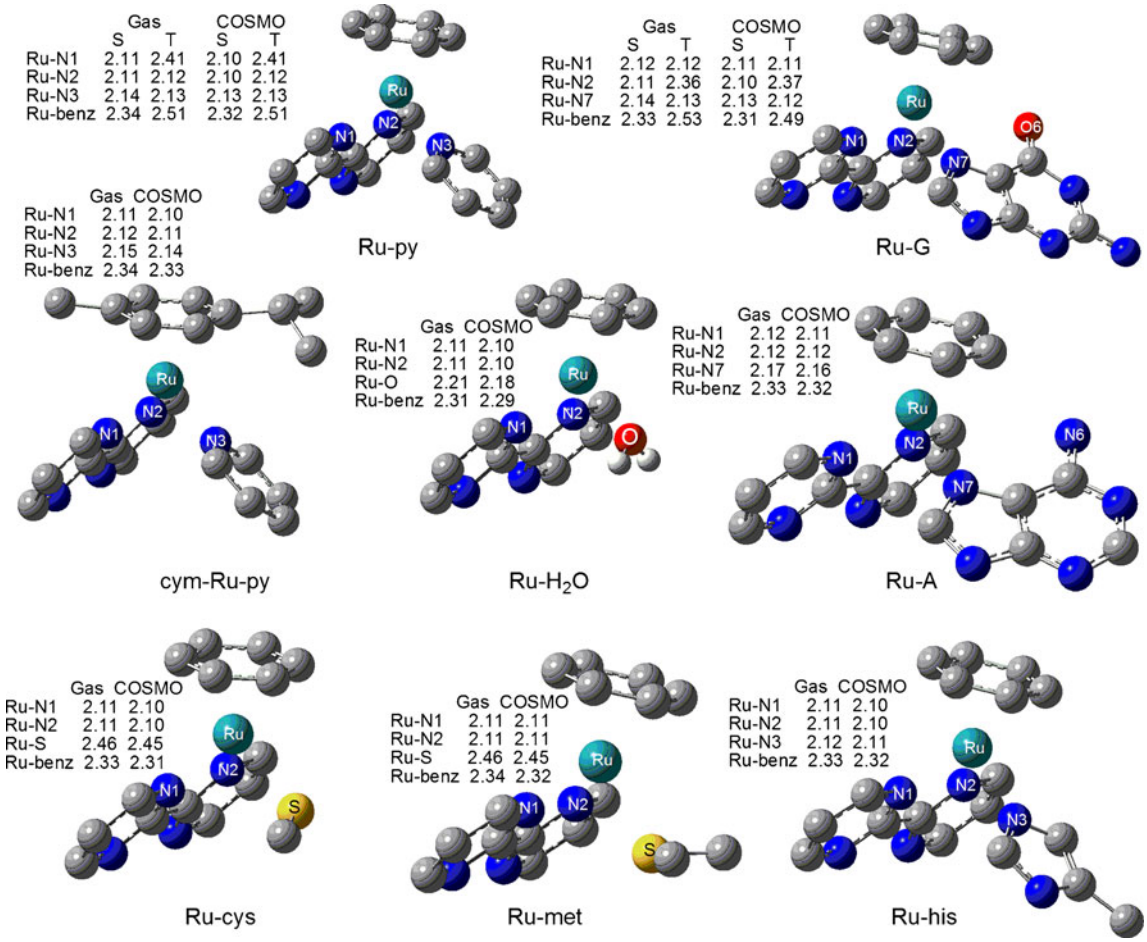

Fig. 2 Geometry parameters of $[(\eta^6\text{-benz})Ru(bpm)L]^{2+}$ complexes. *S* represents the singlet state and *T* the triplet state. Some hydrogen atoms have been omitted for clarity. The distances reported are in angstroms

arene ligands. Overall, the effect of solvent on this system is relatively small, as reflected by the structural characteristics. In the triplet-state structures, Ru-py and Ru-G each have one elongated Ru–N(bpm) bond (from 2.11 to 2.41 Å and from 2.11 to 2.36 Å for Ru-py and Ru-G, respectively) in both the gas phase and aqueous solution. However, the dissociation of bpm is prevented by the strong coordination of the other pyrazine ring of the ligand. Note that, in the optimized geometry of the triplet state, the singlet ground state is still lower in energy by 5.1 kcal mol^{-1}.

Activation of the Ru(II) complex: aquation reaction

To characterize the singlet and triplet excited states of the complex and to obtain insights into the mechanism of ligand photodissociation, a complete set of DFT and TDDFT calculations was performed with Gaussian09 for the complex at the B3LYP/6-31 G** (LanL2DZ for Ru) level.

Upon inspecting the frontier orbitals of Ru-py (Fig. 3), it is clear that the highest occupied molecular orbital (HOMO) and HOMO-1 are almost degenerate and are basically ruthenium-centered (~68 %), with limited contributions from the peripheral ligands. The lowest unoccupied molecular orbital (LUMO) is localized on the bpm ligand (91 %), LUMO+2 is mainly localized on Ru and the bpm ligand, while LUMO+3 is mainly localized on Ru and the benz ligand. LUMO+2 and LUMO+3, which are nearly degenerate, have σ-antibonding character toward py (contribution ~10 %). As shown in Fig. 4, the computed spectrum of cym-Ru-py is in good agreement with the corresponding experimental spectrum (the deviation of the maxima is less than 6 nm, as presented in Table 1), as well as the theoretical data presented by Sadler, since the exact same method was used [25]. The UV spectrum of Ru-py (Fig. 4c) is quite similar to that of cym-Ru-py (Fig. 4b), as the strong transitions are mainly of $d_{Ru} \rightarrow \pi^*_{bpm}$ and $\pi_{arene} \rightarrow \pi^*_{bpm}$ character for both of the complexes (Table 1 and Table S1 of the ESM). Here, we concentrate on the photophysical and photochemical properties of Ru-py.

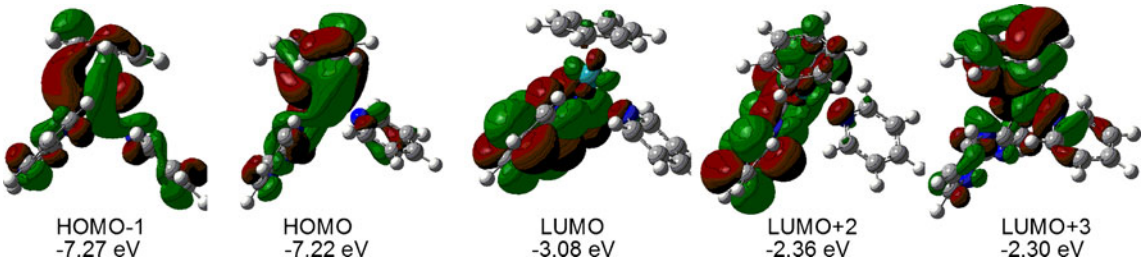

Fig. 3 Some related frontier molecular orbital contour plots of Ru-py

In the UV spectrum of Ru-py (Fig. 4c), two strong transitions with f>0.10 lie in the range 225–300 nm. One is at 260 nm (f=0.13), has obvious ^{1}MLCT character, and mainly originates from HOMO-1→LUMO+6 ($d_{Ru}\rightarrow\pi^*_{benz}$) transitions (Fig. S1). The second is at 256 nm (f=0.22), and has ^{1}LL character. It mainly originates from HOMO-5→LUMO+2 ($\pi_{bpm}\rightarrow\pi^*_{bpm}$) transitions. The long tail of the absorption band in the region 325–400 nm contains two transitions with relatively low intensities. One is at 366 nm (f=0.03), has ^{1}MLCT character, and mainly originates from a HOMO-1→LUMO ($d_{Ru}\rightarrow\pi^*_{bpm}$) transition; the other is at 334 nm (f=0.01), and originates from a HOMO-2→LUMO ($d_{Ru}\rightarrow\pi^*_{bpm}$) transition. Many low ^{1}MLCT states (such as S1, S2, and S3) in the complexes are dissociative toward the py ligand due to the contributions of the LUMO+3 orbital (Table 1), which is of Ru–N3(py) σ*-antibonding character and can be populated by photoexcitation. Although the oscillator strength is zero for S1 in the ground-state absorption spectrum, it becomes non-negligible along the reaction coordinate as the Ru–N3(py) bond increases. These lower-energy singlet transitions (S1, S2, and S3) are energetically available during the photodissociation process at the equilibrium geometry, which may account for the observed photoinduced aquation of the complex, even when the applied excitation wavelength (visible white light, 400–600 nm, 1 Jcm^{-2} h^{-1}) is far from the absorption maximum (254 nm) [25].

To identify the relevant excited states for the photodissociation of the Ru–N3(py) bond, the evolution of the singlet (S1–S4) and triplet (T1–T4) excited states was monitored along the Ru–N3(py) reaction coordinate based on the constrained ground-state geometries, as shown in Fig. 5 and Fig. S3 of the ESM. Though the presence of avoided crossings and our choice of geometry constraint complicates the interpretation of Fig. 5, the slopes of the potential energy curves (PECs) of the singlet excited states S1–S3 along the Ru–N3(py) reaction coordinate indicates that the dissociation of pyridine is facilitated. Coordination of a solvent molecule may follow the photoelimination of the py ligand. The PECs of four triplets (T1–T4) along the Ru–N3(py) reaction coordinate were analyzed as well, as depicted in Fig. 5b. Some of the triplet states in the 400–600 nm region (T1 and T4) have dissociative character because of the

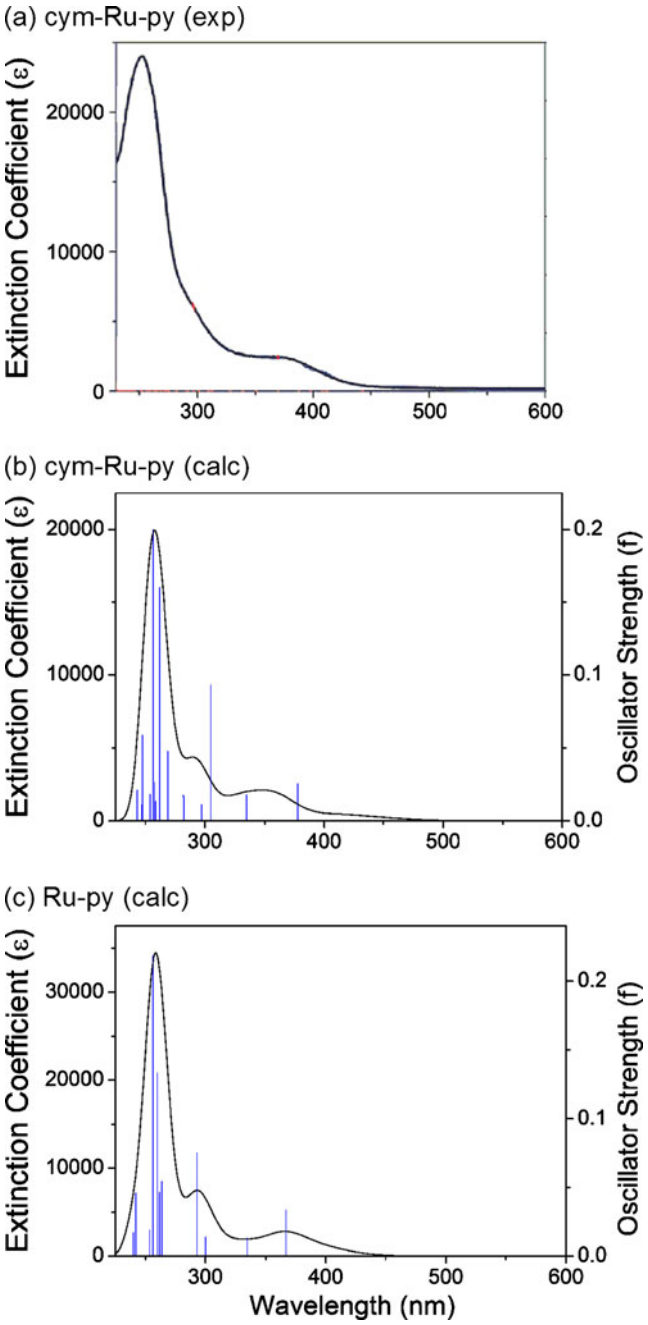

Fig. 4a–c Experimental UV-vis spectrum of cym-Ru-py (**a**) [25], and theoretical UV–vis spectra of cym-Ru-py (**b**) and Ru-py (**c**) in water solution

Table 1 TDDFT singlet transitions for the complex $[(\eta^6\text{-benz})Ru(bpm)(py)]^{2+}$

No.	Energy (eV)	Wavelength (nm)	Osc. strength	Major contributions	Character
1	2.94	422.37	0.0000	HOMO→LUMO+3 (46 %), HOMO-1→LUMO+1 (26 %)	MLCT
2	3.07	404.25	0.0064	HOMO→LUMO+1 (37 %), HOMO-2→LUMO+3 (20 %), HOMO-1→LUMO+3 (21 %)	MLCT
3	3.12	397.31	0.0036	HOMO-1→LUMO+3 (45 %), HOMO-1→LUMO (12 %)	MLCT
4	3.17	391.73	0.0008	HOMO-2→LUMO+1 (52 %), HOMO-2→LUMO+4 (14 %)	MLCT
5	3.25	380.99	0.0005	HOMO→LUMO (79 %)	MLCT
6	3.38	366.29	0.0335	HOMO-1→LUMO (77 %)	MLCT
7	3.60	344.68	0.0019	HOMO-2→LUMO+1 (12 %), HOMO-1→LUMO+1 (38 %)	MLLCT
8	3.70	334.83	0.0130	HOMO-2→LUMO (65 %)	MLCT
9	3.84	323.13	0.0083	HOMO-2→LUMO+3 (54 %)	MLCT
10	4.02	308.41	0.0063	HOMO→LUMO+2 (83 %)	MLCT
11	4.09	303.17	0.0024	HOMO-5→LUMO (43 %)	LL
12	4.13	299.85	0.0136	HOMO-1→LUMO+2 (83 %)	MLCT
13	4.23	292.77	0.0752	HOMO→LUMO+4 (69 %)	MLCT
14	4.27	290.67	0.0029	HOMO-3→LUMO (30 %), HOMO-1→LUMO+4 (53 %)	MLCT
15	4.28	289.74	0.0044	HOMO-3→LUMO (63 %)	LL
16	4.47	277.11	0.0060	HOMO-6→LUMO (80 %)	MLCT
17	4.53	273.66	0.0066	HOMO-2→LUMO+2 (80 %)	MLCT
18	4.57	271.58	0.0001	HOMO→LUMO+5 (97 %)	MLCT
19	4.61	268.89	0.0017	HOMO→LUMO+7 (80 %)	MLCT
20	4.64	267.17	0.0059	HOMO-2→LUMO+4 (63 %)	MLCT
21	4.71	263.51	0.0543	HOMO-1→LUMO+5 (67 %)	MLCT
22	4.72	262.61	0.0079	HOMO-1→LUMO+5 (26 %), HOMO-1→LUMO+7 (25 %), HOMO→LUMO+6 (35 %)	MLCT
23	4.74	261.69	0.0464	HOMO-1→LUMO+6 (46 %)	MLCT
24	4.77	260.00	0.1332	HOMO-1→LUMO+6 (27 %)	MLCT
25	4.84	256.07	0.2181	HOMO-5→LUMO (17 %), HOMO-5→LUMO+2 (21 %)	LL
26	4.89	253.53	0.0190	HOMO-6→LUMO+2 (15 %), HOMO-3→LUMO+1 (41 %)	LL
27	4.91	252.58	0.0067	HOMO-3→LUMO+2 (21 %), HOMO-3→LUMO+3 (73 %)	LMCT
28	4.92	252.20	0.0042	HOMO-3→LUMO+1 (54 %)	LMCT
29	5.04	246.08	0.0004	HOMO-3→LUMO+2 (72 %)	LMCT
30	5.07	244.33	0.0019	HOMO-7→LUMO (78 %)	LMCT
31	5.13	241.86	0.0458	HOMO-2→LUMO+5 (73 %)	MLCT
32	5.17	239.98	0.0169	HOMO-2→LUMO+7 (29 %)	LL

dominant contribution of excitations to LUMO+3 (Table 2). Furthermore, the singlet occupied molecular orbital (SOMO) (Fig. S2 of the ESM) in the optimized lowest-lying triplet-state geometry of Ru-py has strong antibonding character with respect to Ru–N3 (σ*-bond). These results are in agreement with the release of free pyridine upon irradiation with visible light, as detected by ^{1}H NMR [26].

The energy profile for the replacement of the py ligand with a water molecule in Ru-py was also evaluated under standard conditions. Figure 6 displays the optimized geometries and relative energies for the hydration reaction with pertinent geometrical parameters. In the optimized reactant structure (RC), the incoming water interacts with the hydrogen atom of bpm to form a weak hydrogen bond at 2.20 Å. In the TS, the incoming water molecule approaches the metal center, with the Ru–O(water) distance decreasing from 4.72 to 2.82 Å. Also, the adjacent pyridine Ru–N3 bond distance increases from 2.13 to 2.95 Å. In the optimized product structure (PC), the incoming water has replaced the py ligand. In both the TS and the PC, the leaving py is close to the incoming water molecule, which attracts its positively charged hydrogen atom and prompts the formation of a strong hydrogen bond. The calculated activation free energy for the dissociation of the py ligand is 29.8 kcal mol^{-1} in aqueous solution without irradiation. The reaction is endothermic by 5.1 kcal mol^{-1}, as shown in Fig. 6. The high free-energy barrier and endothermicity suggest that the reaction is unlikely to occur under normal

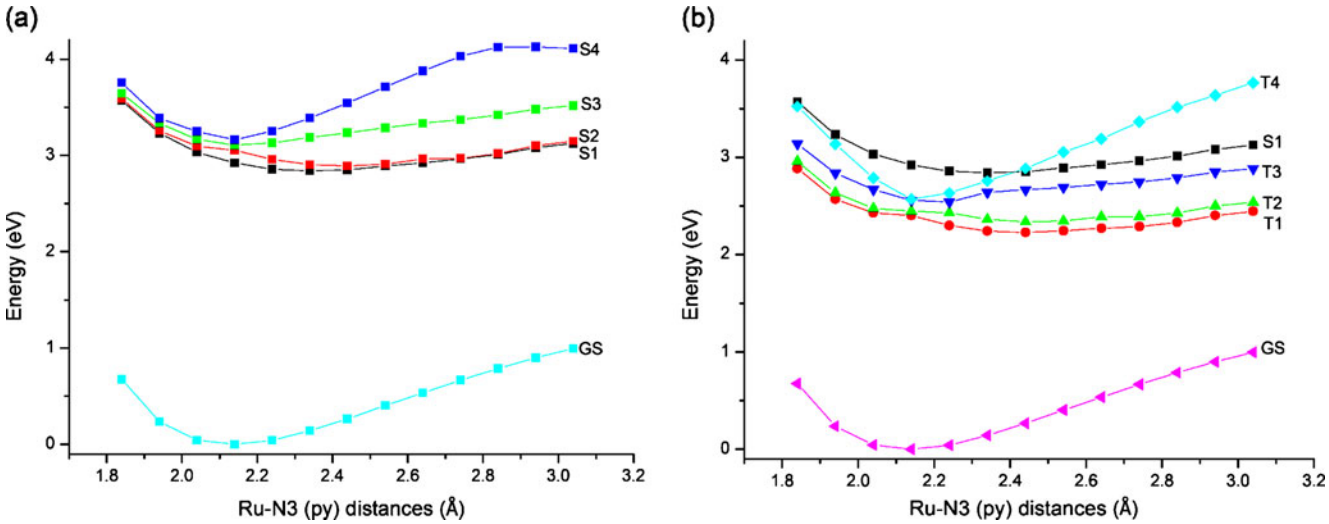

Fig. 5a–b Potential energy curves of the four lowest-energy singlet (**a**) and triplet (**b**) excited states along the Ru–N3(py) coordinate in Ru-py. The zero point of the energy scale is set to be the ground-state (*GS*) energy at its equilibrium geometry

conditions. This is in agreement with the experimental observation that solutions of Ru-py in the dark at 310 K did not show any detectable formation of aqua adducts after 12 h [25, 26].

Interactions of the Ru^{II} arene complexes with biomolecules

After the hydrolysis of the Ru^{II} arene complex, the reactive species Ru–H_2O can bind to DNA [25, 26]. Chemical and spectroscopic studies reveal that this complex exhibits a preference for G over other nucleobases and biomolecules [26]. Moreover, photoreactions of Ru-H_2O with a peptide-oligonucleotide hybrid, Phac-His-Gly-Met-linker-$p^{5'}$dCATGGCT, led to arene release and to guanine adducts, including a GG chelate [26]. The lack of interaction with the peptide fragment confirms the preference of the complex for guanine over other potential biological ligands, such as histidine or methionine. There have been several theoretical investigations into the competitive reactions of Pt^{II} complexes with N-donor (G^{N7}-DNA) and S-donor (thiol/thioether) ligands [45–48]. However, reactions of Ru^{II}-arene anticancer complexes with S-donor amino acids or peptides have not yet been explored, although work has been done to analyze the selectivity between G and A for [(η^6-arene)Ru(en)Cl]$^{2+}$ (en=ethylenediamine) complexes [27, 49, 50]. This section focuses on competitive reactions of the Ru^{II} anticancer complex with model biological molecules, such as G, A, hist, cys, or met.

We first explored the binding energies for the interaction of the benz ligand in the various adducts and conformers with the Ru^{II} cation with various individual neutral ligands, such as H_2O, py, G(N7), A (N7), hist, cys, and met. Binding to O6(G) and N1(A) were not considered, since these atoms are strongly involved in base pairing in DNA. Table 3 summarizes the binding energies for the Ru–L and Ru–benz bonds in [(η^6-benz)Ru(bpm)L]$^{2+}$ complexes, evaluated according to Eqs. 1 and 2. Although the prediction of solvation free energies is inherently problematic for highly

Table 2 TDDFT triplet transitions for the complex [(η^6-benz)Ru(bpm)(py)]$^{2+}$

No.	Energy (eV)	Wavelength (nm)	Osc. strength	Major contributions	Character
1	2.42	513.28	0.0	HOMO-1→LUMO+1 (24 %), HOMO→LUMO+3 (53 %)	MLCT
2	2.45	506.94	0.0	HOMO→LUMO+1 (68 %), HOMO→LUMO+4 (20 %)	MLCT
3	2.57	483.29	0.0	HOMO-1→LUMO+1 (36 %), HOMO-1→LUMO+4 (10 %), HOMO→LUMO+3 (−23 %)	MLCT
4	2.59	477.89	0.0	HOMO-1→LUMO+3 (79 %)	MLCT
5	2.77	447.97	0.0	HOMO-2→LUMO+1 (53 %), HOMO-2→LUMO+4 (16 %), HOMO-1→LUMO+1 (13 %)	MLCT
6	2.92	424.02	0.0	HOMO-2→LUMO+3 (78 %)	MLCT
7	2.96	418.86	0.0	HOMO→LUMO (66 %)	MLCT
8	3.16	392.34	0.0	HOMO-1→LUMO (87 %)	MLCT

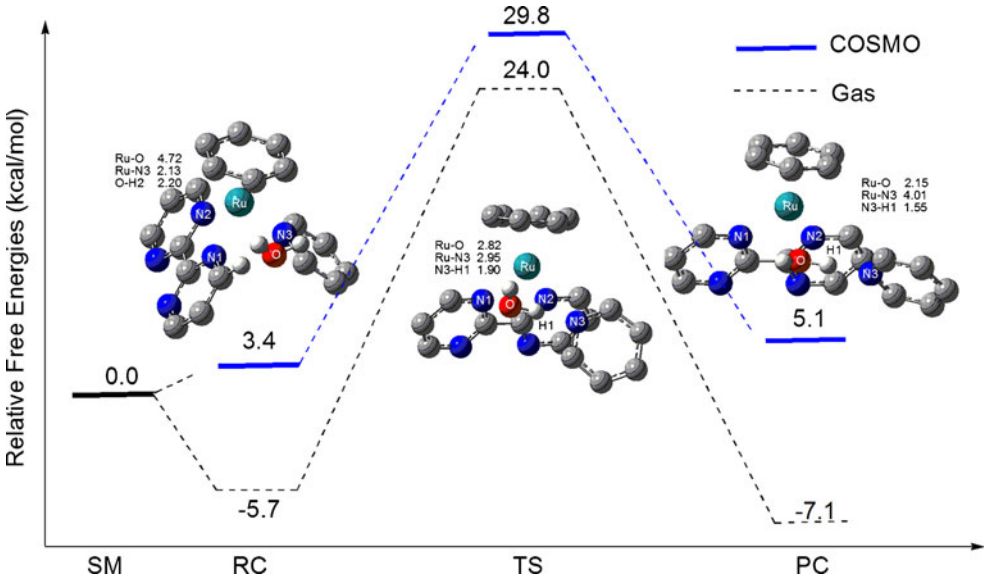

Fig. 6 Free-energy profile of the aquation reaction of $[(\eta^6\text{-benz})Ru(bpm)(py)]^{2+}$ in the gas-phase (*dashed black line*) and the COSMO (*blue solid line*) models in the dark. *SM* refers to Ru-py+H_2O. Some hydrogen atoms have been omitted for clarity. The distances reported are in angstroms

charged species [50, 51], this study focused on their relative differences, since all of these models carry a molecular charge of 2+ in the singlet electronic state. It can be noticed that the binding of the benz to the Ru^{II} cation is significantly weaker for Ru-G and Ru-A adducts (~10 kcal mol^{-1}) compared to other complexes (25.5–34.5 kcal mol^{-1}), indicating that the benz is more labile in Ru-G and Ru-A adducts. Upon inspecting the structures of the optimized fragments, remarkable geometrical rearrangements are observed in the $[Ru(bpm)G]^{2+}$ and $[Ru(bpm)A]^{2+}$ fragments (Fig. S4 of the ESM), in which the G and A change from N7(G or A) coordination to bidentate coordination with O6–Ru–N7 in $[Ru(bpm)G]^{2+}$ and N6–Ru–N7 in $[Ru(bpm)A]^{2+}$, respectively. The tendency of G to participate in bidentate coordination partly contributes to the loss of the arene from monofunctional guanine adducts upon irradiation [26]. The binding energies of Ru-L in solution show the following trend: hist>G (N7)>py>H_2O≈met>A (N7)≈cys. A(N7), cys, and met all show lower binding energies to Ru^{II} than H_2O in aqueous solution, consistent with experimental evidence that the binding of the aquated complex to these sites is not preferred [26]. On the other hand, the binding energies for hist, G (N7), and py are much larger than H_2O, suggesting that these binding sites are favored for the aquated complex. It should be noted that the Ru center binds to hist a little more strongly than guanine by 3.2 kcal mol^{-1}. Experimentally, no interaction of the Ru^{II} arene complex with the peptide fragment, including histidine, has been observed, even in the adduct from which the arene ligand had been lost [26]. However, binding to biomolecules is controlled not only by the thermodynamics but also to a large degree by kinetic factors. We will now focus on the kinetic factors that influence the preference of this Ru^{II} arene complex for guanines on DNA (or RNA) over other potential biological ligands.

To clarify which biomolecules displace the water molecule most easily from the metal, we predicted the reaction free energies and activation free energies for nucleophilic substitution of the water by various nucleophiles. The fully optimized structures for the transition states of these reactions of Ru-H_2O in water are shown in Fig. 7, and the calculated relative free energies of the stationary points in aqueous solution are displayed in Fig. 8.

A dominant preference for initial attack at the N7 position of guanine (G) has been established experimentally, and the further formation of multidentate guanine bases is expected to alter the structure of the DNA (or RNA) dramatically, thus interfering with cell repair mechanisms [26]. As shown in Fig. 7, the G molecule lies 4.15 Å away from the ruthenium atom, with N7 of G forming an H-bond with

Table 3 Binding energies (in kcal mol^{-1}) for the Ru–L and Ru–benz bonds in $[(\eta^6\text{-benz})Ru(bpm)L]^{2+}$ complexes in aqueous solution

Complex	Ru-H_2O		Ru-py		Ru-cys		Ru-met		Ru-his		Ru-G		Ru-A	
Ligand	H_2O	benz	py	benz	cys	benz	met	benz	his	benz	G(N7)	benz	A(N7)	benz
$\Delta E_{(aq)}^{298}$	17.0	46.0	31.7	38.3	24.8	40.2	28.1	37.5	35.3	38.0	31.1	23.9	23.8	23.3
$\Delta H_{(aq)}^{298}$	18.0	45.9	31.7	38.3	25.2	40.4	28.7	38.1	35.3	38.0	31.0	24.0	23.7	23.1
$\Delta G_{(aq)}^{298}$	6.9	32.8	18.9	25.5	12.2	26.5	13.9	22.6	22.3	24.6	16.9	10.3	9.5	10.0

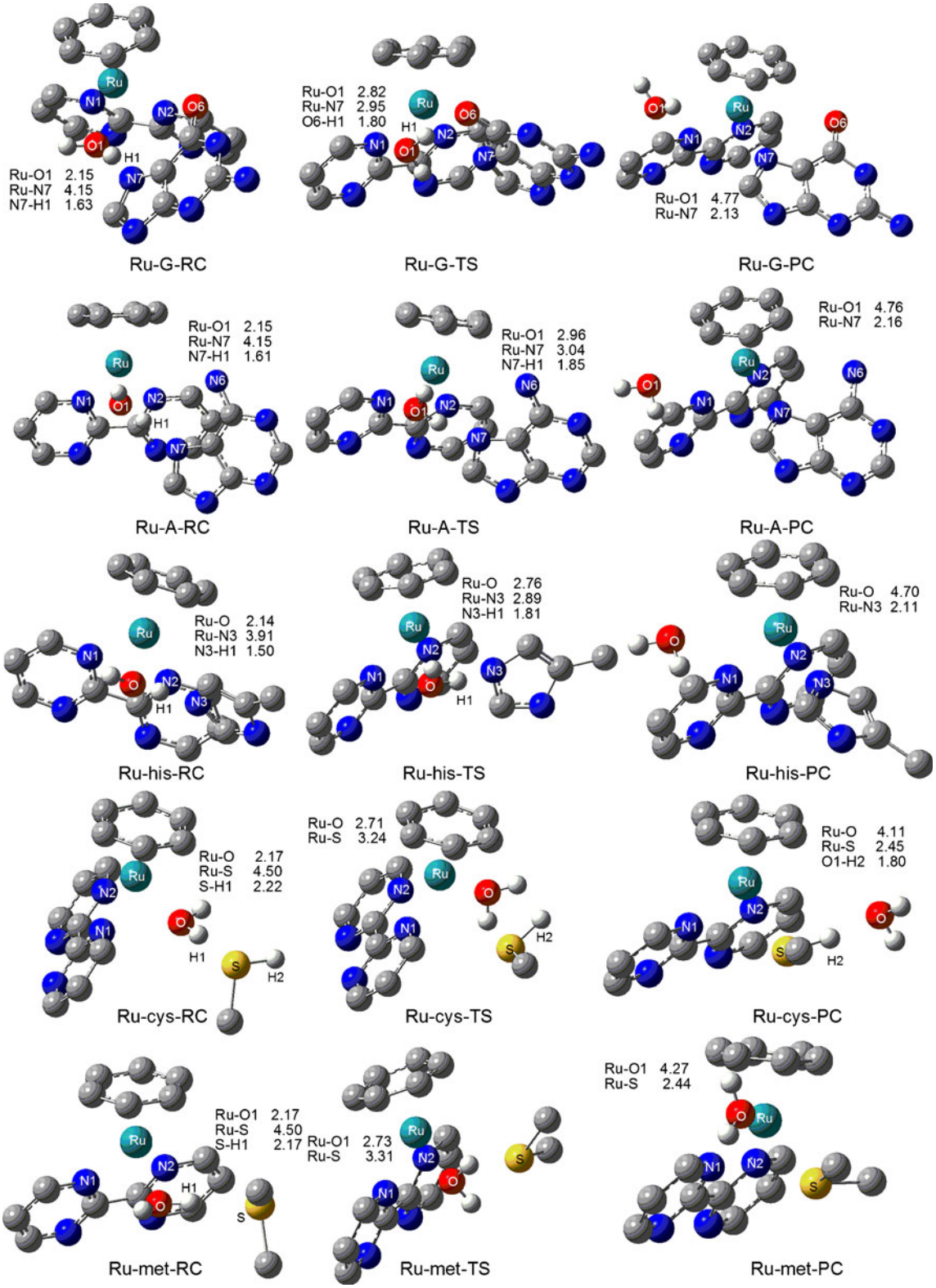

Fig. 7 Optimized structures for biomolecular substitution of water. Some hydrogen atoms are omitted for clarity. The distances reported are in angstroms

the hydrogen of the coordinated water ($R_{N7–H1}$=1.63 Å). As the G molecule approaches the Ru center, the Ru–O1(water) bond distance starts to increase until the transition-state geometry is reached, in which the hydrogen bond between N7 and H1 in the reactant is broken to form another one between O6 and H1 ($R_{O6–H1}$=1.80 Å). The Ru–N7 bond

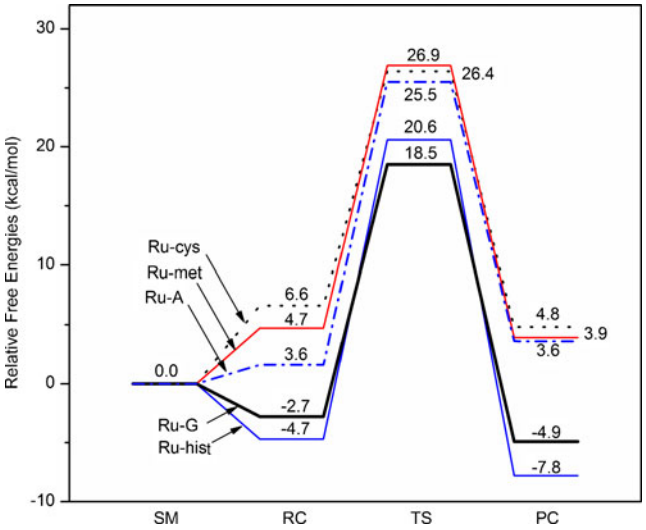

Fig. 8 Free-energy profile for the reactions of Ru-H_2O with various biomolecules. *SM*refers to Ru-H_2O+L

distance in solvent is 2.95 Å. The imaginary frequency observed in the transition state is about 118i cm^{-1} in solvent, and analysis of this vibrational mode clearly indicates the rupture of the Ru–O1(water) bond and the simultaneous formation of the Ru–N7(G) bond. The free-energy barrier is predicted to be 21.3 kcal mol^{-1} for binding to G (N7), with an exothermicity of 4.9 kcal mol^{-1}, indicating that binding to G is facilitated. Replacement by adenine (A) exhibits the similar geometric features to that by G. In the RC structure, the A molecule approaches the ruthenium center to a distance of 4.15 Å, which becomes 3.04 Å in the TS and 2.16 Å in the PC. The imaginary frequency for the transition state corresponding to the scission of the Ru–O1(water) bond and the formation of the Ru–N7(A) bond is 109i cm^{-1} in solvent. The reaction of Ru-H_2O with A (N7) exhibits an activation free-energy barrier of 25.5 kcal mol^{-1}, and the reaction is endothermic by 3.6 kcal mol^{-1}, suggesting that binding to A is not a favorable process.

Next, the reactions with peptide models were examined. In solution, the incoming hist molecule in the RC lies 3.91 Å from the ruthenium center. The hist then approaches the metal, and the transition-state geometry (149i cm^{-1}) is reached with a Ru–N3 distance of 2.89 Å and a Ru–O (water) distance of 3.06 Å. Replacement by hist required a free-energy barrier of 25.3 kcal mol^{-1}, 4 kcal mol^{-1} higher than that for replacement by G (N7), and it was exothermic by 7.8 kcal mol^{-1}. The 4 kcal mol^{-1} difference between the activation barriers to replacement by hist and G (N7) translates into a reaction rate ratio of about three orders of magnitude. Thus, the reaction ultimately affords the G (N7) adduct. Sulfur atoms of cysteine or methionine residues are the most frequently studied binding sites of proteins for Ru-arene complexes [22, 26, 52]. In the reactions of Ru-H_2O with cys and met, the activation energy for substitution by cys, ~26 kcal mol^{-1}, is almost equivalent to that for substitution by met, and both of the processes are endothermic by 4 kcal mol^{-1}, suggesting that binding to S-donor sites is both kinetically and thermodynamically unfavorable compared to G (N7). The Ru–O(water) and Ru–S distances in the transition state of met are a little longer than those in the transition state of cys, and this can be ascribed to the steric hindrance induced by the additional methyl substitute of met compared with cys. The transition states of cys and met have imaginary frequencies of about 122i cm^{-1} and 107i cm^{-1}, respectively, corresponding to the scission of the Ru–O(water) bond and the formation of the Ru–S bond.

As shown by the reaction free-energy profile in Fig. 8, the activation barriers to the reactions of biomolecules with Ru-H_2O show the following trend: G (N7)>hist (N3)≈A (N7)>cys≈met. Moreover, while the reactions with both G (N7) and hist (N3) were predicted to be exothermic, the reactions with cys, met, and A (N7) were found to be slightly endothermic (by about 4 kcal mol^{-1}), indicating that these reactions are also thermodynamically unfavorable. Although the exothermicity for hist (N3) is larger than that of G (N7) by 2.9 kcal mol^{-1}, the activation barrier of G (N7) is significantly lower than that of hist (N3) by 4.1 kcal mol^{-1}. Consequently, binding to G (N7) is the kinetically preferred reaction. The calculated results are consistent with the experimental data, which indicate that the complex prefers G on DNA over other potential biological ligands, such as histidine or methionine amino acids [26]. Although the previous study suggested that this preference resulted from steric hindrance due to the covalent bond between the peptide and the oligonucleotide chain, our calculation indicated that the much lower activation barrier to substitution by G (N7) rather than other biomolecules also supports the predominance of G (N7) binding in the Ru-arene complex.

Conclusions

In summary, DFT and TDDFT calculations combined with the COSMO approach have allowed us to characterize the photochemical properties of photocontrolled Ru-arene complexes and their reactivities with biomolecules. PECs calculated for the elongation of Ru–N3(py) bond gave useful insights into the photodissociation mechanism. Upon irradiation, it is apparent that the dissociation of the py ligand is facilitated. Without photoexcitation, the aquation process required a prohibitively high activation free energy of 29.8 kcal mol^{-1}. This suggests that aquation is unlikely to occur without irradiation, which is in agreement with experimental observations. The binding energies of the benz in the Ru-G and Ru-A adducts are much lower than those

observed for other complexes, suggesting that benz is more labile in these complexes, which partly explains the arene loss exhibited by monofunctional guanine adducts upon irradiation [26]. A (N7), cys, and met show lower binding energies to Ru^{II} than H_2O in aqueous solution, consistent with experimental evidence that the binding of the aquated complex to these sites is not preferred. However, the binding energy of hist is the largest; it is even larger than G, indicating that the discrepancy may originated from kinetic effects. Therefore, the reaction mechanisms of the aquated Ru complex with various biomolecules were explored. The free-energy profiles show that G (N7) exhibits the lowest free-energy activation barrier (21.3 kcal mol^{-1}) among all of the biomolecules investigated. Although the previous study suggested that this preference resulted from the steric hindrance due to the covalent bond between the peptide and the oligonucleotide chain, our calculated results indicate that the much lower activation barrier to substitution by G (N7) rather than other biomolecules also contributes to the predominance of G (N7) binding in the photoactivated Ru-arene complex.

Acknowledgments This work was supported by the National Natural Science Foundation of China (nos. 20725103, 20831006, 20821001, 20973204, 21172274, 21173273), the Guangdong Provincial Natural Science Foundation (no. 9351027501000003), and the National Basic Research Program of China (973, program no. 2007CB815306). It was partially sponsored by the high-performance grid computing platform of Sun Yat-sen University.

References

1. Reedijk J (2009) Platinum anticancer coordination compounds: study of DNA binding inspires new drug design. Eur J Inorg Chem 1303–1312
2. Reedijk J (2011) Increased understanding of platinum anticancer chemistry. Pure Appl Chem 83:1709–1719
3. Bruijnincx PCA, Sadler PJ (2009) Controlling platinum, ruthenium, and osmium reactivity for anticancer drug design. Adv Inorg Chem 61:1–62
4. Crespy D, Landfester K, Schubert US, Schiller A (2010) Potential photoactivated metallopharmaceuticals: from active molecules to supported drugs. Chem Commun 46:6651–6662
5. Mackay FS, Woods JA, Heringova P, Kasparkova J, Pizarro AM, Moggach SA, Parsons S, Brabec V, Sadler PJ (2007) A potent cytotoxic photoactivated platinum complex. Proc Natl Acad Sci USA 104:20743–20748
6. Ronconi L, Sadler PJ (2011) Photoreaction pathways for the anticancer complex *trans*,*trans*,*trans*-$[Pt(N_3)_2(OH)_2(NH_3)_2]$. Dalton Trans 40:262–268
7. Magennis SW, Habtemariam A, Novakova O, Henry JB, Meier S, Parsons S, Oswald IDH, Brabec V, Sadler PJ (2007) Dual triggering of DNA binding and fluorescence via photoactivation of a dinuclear ruthenium(II) arene complex. Inorg Chem 46:5059–5068
8. Salassa L, Garino C, Salassa G, Nervi C, Gobetto R, Lamberti C, Gianolio D, Bizzarri R, Sadler PJ (2009) Ligand-selective photodissociation from $[Ru(bpy)(4AP)_4]^{2+}$: a spectroscopic and computational study. Inorg Chem 48:1469–1481
9. Morris RE, Aird RE, Murdoch PD, Chen HM, Cummings J, Hughes ND, Parsons S, Parkin A, Boyd G, Jodrell DI, Sadler PJ (2001) Inhibition of cancer cell growth by ruthenium(II) arene complexes. J Med Chem 44:3616–3621
10. Aird RE, Cummings J, Ritchie AA, Muir M, Morris RE, Chen H, Sadler PJ, Jodrell DI (2002) In vitro and in vivo activity and cross resistance profiles of novel ruthenium (II) organometallic arene complexes in human ovarian cancer. Brit J Cancer 86:1652–1657
11. Scolaro C, Bergamo A, Brescacin L, Delfino R, Cocchietto M, Laurenczy G, Geldbach TJ, Sava G, Dyson PJ (2005) In vitro and in vivo evaluation of ruthenium(II)-arene PTA complexes. J Med Chem 48:4161–4171
12. Chatterjee S, Kundu S, Bhattacharyya A, Hartinger CG, Dyson PJ (2008) The ruthenium(II)-arene compound RAPTA-C induces apoptosis in EAC cells through mitochondrial and p53-JNK pathways. J Biol Inorg Chem 13:1149–1155
13. Fetzer L, Boff B, Ali M, Xiangjun M, Collin J-P, Sirlin C, Gaiddon C, Pfeffer M (2011) Library of second-generation cycloruthenated compounds and evaluation of their biological properties as potential anticancer drugs: passing the nanomolar barrier. Dalton Trans 40:8869
14. Atsumi M, González L, Daniel C (2007) Spectroscopy of Ru(II) polypyridyl complexes used as intercalators in DNA: towards a theoretical study of the light switch effect. J Photoch Photobio A 190:310–320
15. Bossert J, Daniel C (2008) Electronic absorption spectroscopy of $[Ru(phen)_2(bpy)]^{2+}$, $[Ru(phen)_2(dmbp)]^{2+}$, $[Ru(tpy)(phen)(CH_3CN)]^{2+}$ and $[Ru(tpy)(dmp)(CH_3CN)]^{2+}$: a theoretical study. Coord Chem Rev 252:2493–2503
16. Gossens C, Tavernelli I, Rothlisberger U (2008) DNA structural distortions induced by ruthenium-arene anticancer compounds. J Am Chem Soc 130:10921–10928
17. Reedijk J (1999) Why does cisplatin reach guanine-N7 with competing S-donor ligands available in the cell? Chem Rev 99:2499–2510
18. Reedijk J (2003) New clues for platinum antitumor chemistry: kinetically controlled metal binding to DNA. Proc Natl Acad Sci USA 100:3611–3616
19. Chen HM, Parkinson JA, Parsons S, Coxall RA, Gould RO, Sadler PJ (2002) Organometallic ruthenium(II) diamine anticancer complexes: arene-nucleobase stacking and stereospecific hydrogen-bonding in guanine adducts. J Am Chem Soc 124:3064–3082
20. Chen HM, Parkinson JA, Morris RE, Sadler PJ (2003) Highly selective binding of organometallic ruthenium ethylenediamine complexes to nucleic acids: novel recognition mechanisms. J Am Chem Soc 125:173–186
21. Novakova O, Chen HM, Vrana O, Rodger A, Sadler PJ, Brabec V (2003) DNA interactions of monofunctional organometallic ruthenium(II) antitumor complexes in cell-free media. Biochemistry 42:11544–11554
22. Wang F, Xu J, Habtemariam A, Bella J, Sadler PJ (2005) Competition between glutathione and guanine for a ruthenium(II) arene anticancer complex: detection of a sulfenato intermediate. J Am Chem Soc 127:17734–17743
23. Petzold H, Xu JJ, Sadler PJ (2008) Metal and ligand control of sulfenate reactivity: arene ruthenium thiolato-mono-S-oxides. Angew Chem Int Edit 47:3008–3011
24. Wang FY, Habtemariam A, van der Geer EPL, Fernandez R, Melchart M, Deeth RJ, Aird R, Guichard S, Fabbiani FPA, Lozano-Casal P, Oswald IDH, Jodrell DI, Parsons S, Sadler PJ (2005) Controlling ligand substitution reactions of organometallic complexes: tuning cancer cell cytotoxicity. Proc Natl Acad Sci USA 102:18269–18274
25. Sadler PJ, Betanzos-Lara S, Salassa L, Habtemariam A (2009) Photocontrolled nucleobase binding to an organometallic Ru(II) arene complex. Chem Commun 6622–6624

26. Barragán F, López-Senín P, Salassa L, Betanzos-Lara S, Habtemariam A, Moreno V, Sadler PJ, Marchán V (2011) Photocontrolled DNA binding of a receptor-targeted organometallic ruthenium(II) complex. J Am Chem Soc 133:14098–14108
27. Futera Z, Klenko J, Sponer JE, Sponer J, Burda JV (2009) Interactions of the "piano-stool" [ruthenium(II)(η^6-arene)(en)Cl]$^+$ complexes with water and nucleobases; ab initio and DFT study. J Comput Chem 30:1758–1770
28. Wang H, DeYonker NJ, Gao H, Ji L, Zhao C, Mao Z-W (2012) Mechanism of aquation and nucleobase binding of ruthenium(II) and osmium(II) arene complexes: a systematic comparison DFT study. J Organomet Chem 704:17–28
29. Pizarro AM, Sadler PJ (2009) Unusual DNA binding modes for metal anticancer complexes. Biochimie 91:1198–1211
30. Chen HM, Parkinson JA, Novakova O, Bella J, Wang FY, Dawson A, Gould R, Parsons S, Brabec V, Sadler PJ (2003) Induced-fit recognition of DNA by organometallic complexes with dynamic stereogenic centers. Proc Natl Acad Sci USA 100:14623–14628
31. Becke AD (1993) Density-functional thermochemistry. III. The role of exact exchange. J Chem Phys 98:5648–5652
32. Lee C, Yang W, Parr RG (1988) Development of the Colle–Salvetti correlation-energy formula into a functional of the electron density. Phys Rev B 37:785–789
33. Dorcier A, Dyson PJ, Gossens C, Rothlisberger U, Scopelliti R, Tavernelli I (2005) Binding of organometallic ruthenium(II) and osmium(II) complexes to an oligonucleotide: a combined mass spectrometric and theoretical study. Organometallics 24:2114–2123
34. Wang HL, DeYonker NJ, Gao H, Tan CP, Zhang XT, Ji LN, Zhao CY, Mao ZW (2012) Aquation and dimerization of osmium(II) anticancer complexes: a density functional theory study. RSC Adv 2:436–446
35. Hay PJ, Wadt WR (1985) Ab initio effective core potentials for molecular calculations. Potentials for the transition metal atoms Sc to Hg. J Chem Phys 82:270–283
36. McLean AD, Chandler GS (1980) Contracted Gaussian basis sets for molecular calculations. I. Second row atoms, Z=11–18. J Chem Phys 72:5639–5648
37. Klamt A (1995) Conductor-like screening model for real solvents: a new approach to the quantitative calculation of solvation phenomena. J Phys Chem 99:2224–2235
38. Klamt A, Schüürmann G (1993) COSMO: A new approach to dielectric screening in solvents with explicit expressions for the screening energy and its gradient. J Chem Soc Perkin Trans 2:799–805
39. Casida ME, Jamorski C, Casida KC, Salahub DR (1998) Molecular excitation energies to high-lying bound states from time-dependent density-functional response theory: characterization and correction of the time-dependent local density approximation ionization threshold. J Chem Phys 108:4439–4449
40. Stratmann RE, Scuseria GE, Frisch MJ (1998) An efficient implementation of time dependent density functional theory for the calculation of excitation energies of large molecules. J Chem Phys 109:8218–8224
41. Salassa L, Garino C, Salassa G, Gobetto R, Nervi C (2008) Mechanism of ligand photodissociation in photoactivable [Ru(bpy)$_2$L$_2$]$^{2+}$complexes: a density functional theory study. J Am Chem Soc 130:9590–9597
42. Salassa L, Garino C, Albertino A, Volpi G, Nervi C, Gobetto R, Hardcastle KI (2008) Computational and spectroscopic studies of new rhenium(I) complexes containing pyridylimidazo[1,5-*a*]pyridine ligands: charge transfer and dual emission by fine-tuning of excited states. Organometallics 27:1427–1435
43. O'Boyle NM, Tenderholt AL, Langner KM (2008) Software news and updates cclib: a library for package-independent computational chemistry algorithms. J Comput Chem 29:839–845
44. Frisch MJ et al (2010) Gaussian 09, revision A.01. Gaussian Inc., Wallingford
45. Zimmermann T, Zeizinger M, Burda JV (2005) Cisplatin interaction with cysteine and methionine, a theoretical DFT study. J Inorg Biochem 99:2184–2196
46. Zimmermann T, Chval Z, Burda JV (2009) Cisplatin interaction with cysteine and methionine in aqueous solution: computational DFT/PCM study. J Phys Chem B 113:3139–3150
47. Deubel DV (2004) Factors governing the kinetic competition of nitrogen and sulfur ligands in cisplatin binding to biological targets. J Am Chem Soc 126:5999–6004
48. Baik MH, Friesner RA, Lippard SJ (2003) Theoretical study of cisplatin binding to purine bases: why does cisplatin prefer guanine over adenine. J Am Chem Soc 125:14082–14092
49. Gossens C, Tavernelli I, Rothlisberger U (2009) Binding of organometallic ruthenium(II) anticancer compounds to nucleobases: a computational study. J Phys Chem A 113:11888–11897
50. Gkionis K, Platts JA, Hill JG (2008) Insights into DNA binding of ruthenium arene complexes: role of hydrogen bonding and pi stacking. Inorg Chem 47:3893–3902
51. Besker N, Coletti C, Marrone A, Re N (2007) Binding of antitumor ruthenium complexes to DNA and proteins: a theoretical approach. J Phys Chem B 111:9955–9964
52. Wang FY, Chen HM, Parkinson JA, Murdoch PD, Sadler PJ (2002) Reactions of a ruthenium(II) arene antitumor complex with cysteine and methionine. Inorg Chem 41:4509–4523